Technical Report

Temporal and Spatial Creep Variability: Detecting Decadal Changes in Fault Behavior in Northern California

SCEC Award # 25123

Investigators: Roland Bürgmann (UCB), Danielle Lindsay (UCB), Taka'aki Taira (UCB)

Project Period: February 1, 2025 – January 31, 2026

Introduction and Motivation

Earthquake potential along faults is not constant through time, but rather a time-dependent process whereby changes in strain accumulation over short (e.g., slow slip events) and long (e.g., viscous relaxation) timescales affect hazard assessment. This project addresses the Rodgers Creek (RC) and Maacama (MA) faults in northern California—lesser-studied segments of the Hayward–RC–MA fault zone that together pose significant seismic risk. Over the past 500 years, a moment deficit sufficient for an *M*w 7.0–7.2 has accumulated on the Maacama Fault, and the Rodgers Creek Fault has similarly accumulated moment for an *M*w 7.1 (Lienkaemper et al., 2014; Schwartz et al., 2014). Characterizing where and how fault creep occurs along these structures is therefore directly relevant to seismic hazard and the earthquake cycle.

Aseismic creep—the gradual sliding of one fault block past another without generating detectable seismic waves—plays a crucial role in determining the seismic hazard of a given fault. Creeping fault segments reduce the energy available for large earthquakes, may act as barriers to rupture propagation, and can exhibit accelerations that increase stressing rates on adjacent locked asperities (Avouac, 2015; Harris, 2017; Kaneko et al., 2010). Changes in creep rate reflect the evolving stress and frictional state of the fault over timescales ranging from seasonal (e.g., pore fluid infiltration from precipitation) to decadal (e.g., viscous relaxation or slow-slip recovery), with direct implications for understanding temporal variability in seismic hazard.

Most existing surface creep measurements along the RC–MA system concentrate on populated areas that host alignment arrays and produce coherent C-band InSAR data. Much of the fault zone lies in densely vegetated terrain where prior InSAR studies have been limited by coherence loss, and no creepmeters have been installed along either fault. By utilizing ALOS-2 L-band InSAR—which maintains coherence through vegetation—together with Sentinel-1 C-band InSAR, terrestrial alignment arrays, and a new catalog of characteristic repeating earthquakes (CREs), this project delivers a spatially continuous and temporally resolved picture of fault creep along the entire RC–MA system. Our work directly addresses SCEC Science Milestones A1-3 (identifying fault zones for further work), A3-5 (geodetic fault slip rates in Northern California), and D1-1 (assessing space- and time-dependent variables influencing seismicity rates).

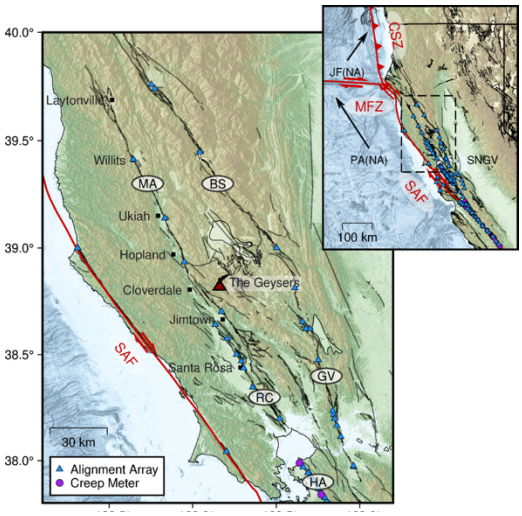

Figure 1. Location of Rodgers Creek and Maacama Faults in Northern California.

The project was organized around two primary objectives: (1) mapping the spatial distribution of surface and shallow creep across the full fault system, and (2) characterizing temporal variability in creep rates at seasonal, annual, and multi-year timescales. For spatial mapping, we ask which segments exhibit active creep, how continuous creep is along strike, and whether multiple fault strands are active. For temporal variability, we ask whether creep rates fluctuate, what mechanisms drive changes, and whether evidence exists for past slow-slip events or sustained creep suppression.

Methods

InSAR Surface Creep Estimates. Surface creep rates were computed from Sentinel-1 and ALOS-2 InSAR time series spanning 2015–2024. ALOS-2 operates at L-band (~24 cm wavelength), providing better coherence in vegetated terrain, while Sentinel-1 at C-band (~5.6 cm wavelength) offers higher precision and more frequent temporal sampling (6–12 day repeat intervals). ALOS-2 ScanSAR interferograms were processed with ISCE-2, including ionospheric corrections and Goldstein-Werner filtering (strength 0.6; multilook factor 10 × 56), yielding an 160 m square pixel size. Displacement time series were inverted with MintPy, with corrections for tropospheric delay, solid earth tides, and DEM error; pixels with temporal coherence below 0.7 were masked. Sentinel-1 interferograms were generated through the ASF HyP3 cloud-based service at ~80 m pixel resolution.

At 250 m increments along remapped fault traces, 500 m-wide fault-perpendicular profiles were extracted to estimate fault-parallel creep rates. For ALOS-2 descending-only data, line-of-sight displacements were projected into the fault-parallel direction using local incidence angle, satellite azimuth, and fault strike. For Sentinel-1, ascending and descending time series were decomposed into vertical and fault-parallel components at each time step. Sentinel-1 time series were fit with a combined linear and seasonal model, resolving long-term rates and seasonal amplitudes simultaneously.

Characteristic Repeating Earthquake (CRE) Catalog. A new CRE catalog was assembled for the RC–MA zone covering 1984–2020, expanding prior efforts northward. We analyzed waveforms for 71,297 earthquakes with $M \geq 1.0$ from the Northern California Seismic System catalog, computing vertical-component waveform coherency at 8–24 Hz in a 10.24 s window from the direct P onset. At coherency thresholds of 0.95–0.97, we detected 220–429 CREs within 95–184 families. Slip for each event was inferred from magnitude using empirical scaling (Nadeau and Johnson, 1998). Cumulative fault slip per segment was tracked over time as a proxy for shallow creep rate changes, following the averaging approach of Nadeau and McEvilly (2004).

Alignment Arrays. Long-running alignment array records from the USGS were analyzed, focusing on MWIL in Willits (1991–2022, 158 mm cumulative displacement) and MUKI in Ukiah (1993–2021, 125 mm cumulative displacement). Both sites were occupied 4–5 times per year before 2008 and annually thereafter. We differentiated cumulative displacement to obtain instantaneous velocities, performed piecewise linear regression to identify rate changes and discrete slip steps, and fit harmonic seasonal models to resolve annual periodicity in creep rates.

Results

Spatial Distribution of Creep. Surface creep along the Rodgers Creek Fault initiates south of Santa Rosa, remains steady at 3–4 mm/yr, and ceases northward near the RCBP alignment array.

ALOS-2 InSAR shows a clear velocity step along the fault trace near alignment array RCMW in Santa Rosa. The shallowest CREs (~2 km depth) correlate spatially with peak slip rates from both InSAR and the alignment array, confirming that surface creep, CRE distribution, and shallow fault behavior are coupled along-strike. The southern RC lacks seismicity, consistent with the interpreted rupture extent of a large earthquake around 1715.

Along the Maacama Fault, surface creep initiates north of Jimtown, varies between 4–8 mm/yr, and ceases north of Willits. Peak rates are observed adjacent to The Geysers geothermal field between Jimtown and Cloverdale, and between Ukiah and Willits along the main fault trace. The envelope of surface creep rates broadly follows the base of the seismogenic zone: where seismicity shallows to ~6 km near Cloverdale—attributable to elevated geothermal gradients from The Geysers raising the brittle-ductile transition—surface creep rates peak. This supports a physically consistent model linking thermal structure, locking depth, and surface creep. CREs and seismicity reveal structural complexity including a pull-apart basin between Cloverdale and Ukiah, and an eastern fault strand near Willits that hosted the 2020 swarm (Shelly et al., 2023) but shows no surface creep. Landslide signals within the 1.5 km sampling aperture locally complicate surface creep estimates near MAMR.

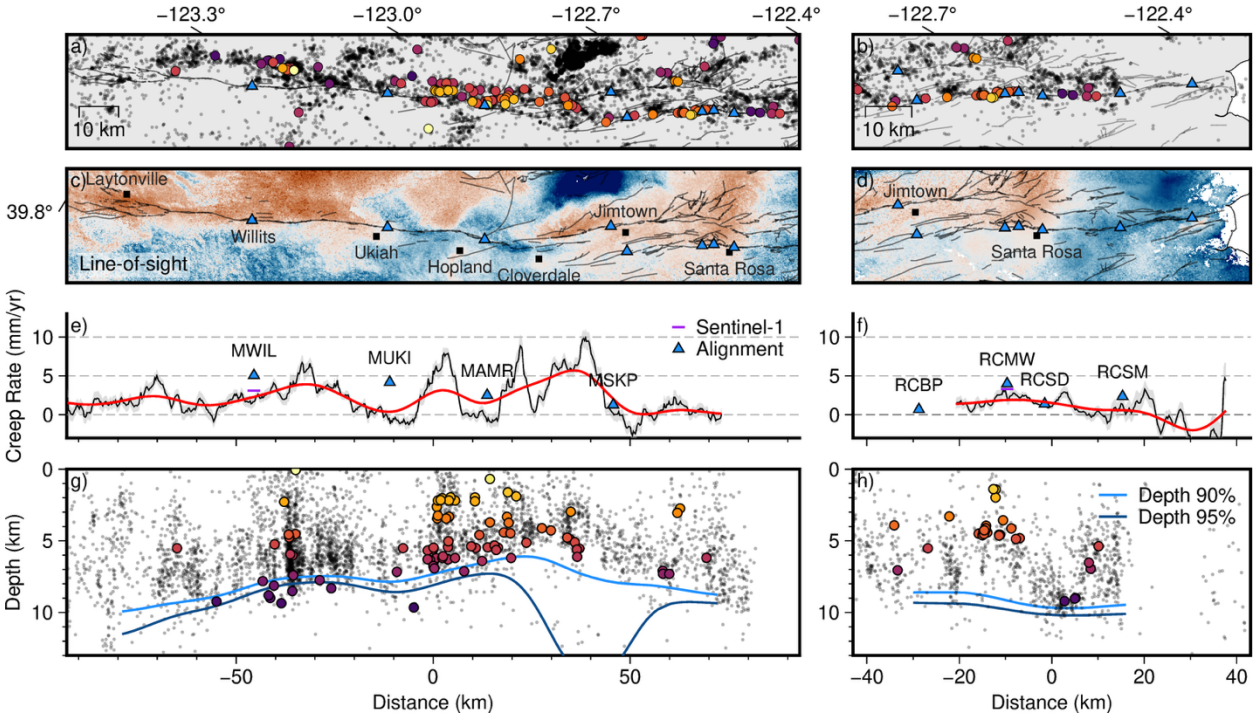

Figure 2.(left) Maacama and (right) Rodgers Creek faults. Maps of (a,b) CREs and background seismicity, (c,d) line-of-sight (LOS) velocity field. (e,f) Surface creep estimates from ALOS-2, Sentinel-1, and alignment arrays. (g,h) Along fault cross-sections with background seismicity, CRE's and depth of 90% and 95% of seismicity.

2002 Creep Event and Decade-long Suppression. The cumulative displacement time series from MWIL shows three discrete creep steps (1994: 6.6 mm; 1996: 4.8 mm; 2002: 5.7 mm) against a long-term average rate of 5.1 ± 0.1 mm/yr. Following the 2002 step, the inter-event rate decreased to 3.65 ± 0.09 mm/yr—a 28% reduction—persisting until ~2014. The MUKI array 32 km to the south recorded a corresponding 8.1 mm step in the following epoch and a rate decrease from 4.4 ± 0.2 to 3.4 ± 0.2 mm/yr.

Three independent lines of evidence confirm this represents a spatially extensive creep event with multi-year recovery. First, the duration of the post-event slowdown far exceeds seasonal or drought cycles, indicating a tectonic origin. Second, the creep event affected both MWIL and MUKI (separated by 32 km), demonstrating spatial coherence over at least that distance. Third, all three independent CRE catalogs show 46–51% reductions in cumulative slip rate on the northern Maacama Fault after 2002, and background seismicity rates decreased by ~20% in the same period. The suppression did not extend to the southern Maacama or Rodgers Creek faults.

Evaluation of potential triggering mechanisms found no compelling candidate. No earthquakes ≥ Mw 4 occurred within 50 km of MWIL during the relevant epoch, and precipitation records indicate average annual rainfall with no anomalous daily intensities. The most parsimonious interpretation is a spontaneous slow-slip event (SSE). Notably, the winter preceding the 2002 event saw near-zero peak creep rates ~146 days before the modeled seasonal peak, suggesting a transient locking period that preceded the larger slip release, consistent with threshold-type behavior (Schulz et al., 1983). The post-event slow decay is reminiscent of fault healing or pore fluid diffusion.

Figure 3. Alignment array time series from Wilitis (MWIL, left) and Ukiah (MUKI, right)(McFarland et al., 2017). (a,b) Displacement time series, with linear velocity, location of identified steps, and interval velocities. (c,d) Detrended displacement time series highlighting creep events and for MWIL a sustained period of creep suppression following the 2002 event. (e,f) Instantaneous velocity with a harmonic model highlighting the seasonality of surface creep rate and mean instantaneous velocity

for each segment. (g) Background seismicity within ± 40\,km of MWIL along the fault zone, with normalized cumulative moment and count (Waldhauser et al., 2009). Note activity related to the 2020 swarm (Shelly et al., 2023). (h) Cumulative and daily precipitation data, along with a harmonic model of daily rainfall (PRISM, 2014).

Seasonal Modulation of Creep. Seasonal modulation of creep rates is evident in both alignment array records and Sentinel-1 InSAR time series. At MWIL, creep rates peak around December 20 (±11 days). The peak velocity precedes peak annual precipitation by ~44 days, while the onset of seasonal rainfall leads the peak creep rate by ~42 days, indicating that surface creep responds to the onset rather than the accumulation of precipitation. This is consistent with pore-fluid pressure increases promoting fault slip (Roeloffs, 2001).

Decomposition of Sentinel-1 ascending and descending time series into vertical and fault-parallel components reveals that the dominant seasonal signal in line-of-sight data is driven by vertical motion, not fault-parallel creep. The vertical signal reflects differential elastic sediment deformation across the fault driven by asymmetric groundwater levels adjacent to subsiding basins (the Little Lake Basin east of Willits; The Geysers to the west). Fault-parallel seasonal amplitudes are comparatively small (0.3–0.73 mm at Willits and Santa Rosa, respectively). These findings underscore that multi-geometry InSAR decomposition is essential: undecomposed LOS time series risk misattributing seasonal vertical signals to fault-parallel creep, biasing surface creep rate estimates.

For the RC in Santa Rosa, Sentinel-1 yields a current creep rate of 4.1 mm/yr, consistent with 4.3 mm/yr at alignment array RCMW. Near MWIL, InSAR yields 3.1 mm/yr—comparable to the post-2002 suppressed rate of 3.7 mm/yr and well below the long-term average of 5.1 mm/yr—suggesting the suppression documented in alignment arrays may persist into the modern InSAR observation period.

Discussion and Conclusions

This study delivers an integrated spatiotemporal characterization of fault creep along the RC–MA fault zone, combining InSAR, alignment arrays, and CREs across multiple timescales. Our results document that fault creep on these moderately loaded faults varies over seasonal to decadal timescales, shaped by evolving stress, hydrological forcing, and internal fault properties—with direct implications for seismic hazard assessment.

The 2002 creep event and subsequent decade-long suppression are the most significant findings of this project period. The coherence of the signal across surface and depth observations, combined with the absence of an identifiable external trigger, favors spontaneous initiation. Post-event creep suppression increases the moment deficit available for future earthquakes; the accompanying decrease in background seismicity is consistent with reduced fault loading during the suppressed period. This behavior—a spontaneous SSE followed by multi-year recovery—has rarely been documented on lower-slip-rate continental strike-slip faults and highlights that temporal variability in seismic hazard is not confined to the heavily monitored creeping San Andreas.

The correlation between surface creep rates and seismogenic depth along the Maacama Fault provides a natural laboratory for testing fault coupling models. The elevated geothermal gradient from The Geysers locally shallows the brittle-ductile transition, reduces seismogenic depth, and produces the observed peak in surface creep rates. This setting offers a rare opportunity to isolate the effect of thermal structure on fault behavior, independent of compositional variability, using the 2D crack framework (Savage and Lisowski, 1993).

Key conclusions: (1) The Rodgers Creek Fault creeps at 3–4 mm/yr near Santa Rosa; the Maacama Fault creeps at 4–8 mm/yr between Jimtown and Willits, with peak rates correlated with shallow seismogenic depth near The Geysers. (2) A creep event in early 2002 was followed by a sustained 28% reduction in surface creep rates at MWIL, corroborated by 46–51% reductions in CRE-inferred seismogenic slip rates on the northern Maacama Fault; no clear triggering mechanism was identified, suggesting spontaneous slow slip. (3) Seasonal modulation of creep responds to the onset rather than peak of annual precipitation, and multi-geometry InSAR decomposition is required to separate vertical and fault-parallel signals. (4) The Maacama Fault's proximity to The Geysers provides a testable physical framework for linking geothermal gradient, seismogenic depth, and surface creep expression.

Data and Code Availability

ALOS-2/PALSAR-2 Level 1.1 SLC products are publicly available via JAXA G-Portal and the NASA/ASF Distributed Active Archive Center; data from 2015–2021 are also archived with the WInSAR Consortium. Sentinel-1 interferograms were produced with the ASF HyP3 service and are freely available. Final analysis code and figures are archived at Lindsay (2025a; doi: 10.5281/zenodo.17298580). InSAR time series and velocity solutions are available at Lindsay (2025b; doi: 10.5281/zenodo.15116865). The CRE catalog is available at Taira (2024; doi: 10.5281/zenodo.14238934). Alignment array data are available through McFarland et al. (2023; doi: 10.5066/F76W9896).

Acknowledgements

This material is based upon work supported by the Southern California Earthquake Center (SCEC) under Award No. 25123 and the U.S. Geological Survey under Grant No. G24AP00049. Danielle Lindsay received support from a NASA FINESST fellowship (80NSSC21K1617) and a Fulbright-EQC award. ALOS-2/PALSAR-2 data were supplied via RA4-PI 1298 and RA6-PI 3311. Computations used the Savio cluster at the University of California, Berkeley. We thank Austin Elliott for guidance on alignment array datasets and Yuexin Li for methodological advice.

References

Avouac, J.-P. (2015). From geodetic imaging of seismic and aseismic fault slip to dynamic modeling of the seismic cycle. Annual Review of Earth and Planetary Sciences, 43(1), 233–271.

Bürgmann, R. (2018). The geophysics, geology and mechanics of slow fault slip. Earth and Planetary Science Letters, 495, 112–134.

Field, E. H., et al. (2014). Uniform California Earthquake Rupture Forecast, version 3 (UCERF3)—The time-independent model. Bulletin of the Seismological Society of America, 104(3), 1122–1180.

Funning, G. J., Bürgmann, R., Ferretti, A., Novali, F., & Fumagalli, A. (2007). Creep on the Rodgers Creek fault, northern San Francisco Bay area from a 10 year PS-InSAR dataset. Geophysical Research Letters, 34(19).

Harris, R. A. (2017). Large earthquakes and creeping faults. Reviews of Geophysics, 55(1), 169–198.

Kaneko, Y., Avouac, J.-P., & Lapusta, N. (2010). Towards inferring earthquake patterns from geodetic observations of interseismic coupling. Nature Geoscience, 3(5), 363–369.

Khoshmanesh, M., & Shirzaei, M. (2018). Episodic creep events on the San Andreas Fault caused by pore pressure variations. Nature Geoscience, 11(8), 610–614.

Li, Y., Bürgmann, R., & Taira, T. (2023). Spatiotemporal variations of surface deformation, shallow creep rate, and slip partitioning between the San Andreas and southern Calaveras Fault. Journal of Geophysical Research: Solid Earth, 128(1), e2022JB025363.

Lienkaemper, J. J., McFarland, F. S., Simpson, R. W., & Caskey, S. J. (2014). Using surface creep rate to infer fraction locked for sections of the San Andreas fault system in northern California. Bulletin of the Seismological Society of America, 104(6), 3094–3114.

Lindsay, D., Bürgmann, R., Materna, K., & Fielding, E. J. (2025). Nine-Year L-band InSAR Time Series of Tectonic and Non-tectonic Surface Deformation in Northern California. ESS Open Archive (preprint). doi: 10.22541/essoar.175647546.63899374/v1.

McFarland, F. S., Lienkaemper, J. J., Caskey, S. J., & Elliott, A. J. (2023). Data from Theodolite Measurements of Creep Rates on San Francisco Bay Region Faults, California (ver. 2.2). U.S. Geological Survey data release. doi: 10.5066/F76W9896.

Murray, J. R., Minson, S. E., & Svarc, J. L. (2014). Slip rates and spatially variable creep on faults of the northern San Andreas system inferred through Bayesian inversion of GPS data. Journal of Geophysical Research: Solid Earth, 119(7), 6023–6047.

Nadeau, R. M., & Johnson, L. R. (1998). Seismological studies at Parkfield VI: Moment release rates and estimates of source parameters for small repeating earthquakes. Bulletin of the Seismological Society of America, 88(3), 790–814.

Nadeau, R. M., & McEvilly, T. V. (2004). Periodic pulsing of characteristic microearthquakes on the San Andreas fault. Science, 303(5655), 220–222.

Prentice, C. S., Larsen, M. C., Kelsey, H. M., & Zachariasen, J. (2014). Late Holocene slip rate and ages of prehistoric earthquakes along the Maacama Fault near Willits, Mendocino County, northern California. Bulletin of the Seismological Society of America, 104(6), 2966–2984.

Roeloffs, E. A. (2001). Creep rate changes at Parkfield, California 1966–1999: Seasonal, precipitation induced, and tectonic. Journal of Geophysical Research: Solid Earth, 106(B8), 16525–16547.

Savage, J., & Lisowski, M. (1993). Inferred depth of creep on the Hayward fault, central California. Journal of Geophysical Research: Solid Earth, 98(B1), 787–793.

Schulz, S., Burford, R. O., & Mavko, B. (1983). Influence of seismicity and rainfall on episodic creep on the San Andreas fault system in central California. Journal of Geophysical Research: Solid Earth, 88(B9), 7475–7484.

Schwartz, D. P., et al. (2014). The earthquake cycle in the San Francisco Bay region: AD 1600–2012. Bulletin of the Seismological Society of America, 104(3), 1299–1328.

Shakibay Senobari, N., & Funning, G. J. (2019). Widespread fault creep in the northern San Francisco Bay Area revealed by multistation cluster detection of repeating earthquakes. Geophysical Research Letters, 46(12), 6425–6434.

Shelly, D. R., Skoumal, R. J., & Hardebeck, J. L. (2023). Fracture-mesh faulting in the swarm-like 2020 Maacama sequence. Geophysical Research Letters, 50(1), e2022GL101233.

Shirzaei, M., & Bürgmann, R. (2013). Time-dependent model of creep on the Hayward fault from joint inversion of 18 years of InSAR and surface creep data. Journal of Geophysical Research: Solid Earth, 118(4), 1733–1746.

Waldhauser, F., & Schaff, D. P. (2021). A comprehensive search for repeating earthquakes in northern California. Journal of Geophysical Research: Solid Earth, 126(11), e2021JB022495.